

FAINT SCATTERING AROUND PULSARS: PROBING THE INTERSTELLAR MEDIUM ON SOLAR SYSTEM SIZE SCALES

D. R. STINEBRING,¹ M. A. McLAUGHLIN,² J. M. CORDES,² K. M. BECKER,¹ J. E. ESPINOZA GOODMAN,¹
M. A. KRAMER,¹ J. L. SHECKARD,¹ AND C. T. SMITH¹

Received 2000 October 2; accepted 2000 December 12; published 2001 February 23

ABSTRACT

We have made high-resolution, high-sensitivity dynamic spectra of a sample of strong pulsars at 430 MHz with the Arecibo radio telescope. For four pulsars we find faint but sharply delineated features in the secondary spectra. These are examples of the previously observed “crisscross” or “multiple drift slope” phenomenon presumed to be due to multiple imaging of the pulsar by the interstellar medium (ISM). The unprecedented resolution and dynamic range of our observations allow a deeper level of analysis. Distances to the dominant scattering screen along the line of sight are determined and are shown to agree well with those inferred from other scintillation phenomena. Multiple imaging of the pulsar by the ISM is required. A compact central image surrounded by a faint scattering halo, roughly circularly symmetric, is consistent with the data. Scattering from filaments may also be consistent. The angular extent of the scattering material parallel to the direction of the pulsar velocity is ~ 5 mas, corresponding to a linear extent of ~ 2 AU. Further observations of these features should allow better discrimination between models and an identification of the scattering structures.

Subject headings: ISM: general — ISM: structure — pulsars: general — techniques: spectroscopic

1. INTRODUCTION

Scattering by density inhomogeneities in the ionized interstellar medium (ISM) causes multiple rays to interfere, producing frequency structure in the spectra of spatially coherent sources such as pulsars (Scheuer 1968; Rickett 1990). The relatively high transverse velocities of most pulsars cause the spectra to change significantly on timescales of minutes to hours. When the spectrum is monitored over time, the resulting two-dimensional array or “dynamic spectrum” is often dominated by a random pattern of scintillation maxima with characteristic bandwidth and timescale (Cordes, Weisberg, & Boriakoff 1985). On occasion, however, more organized features are present. The best studied of these are periodic fringe patterns in the dynamic spectra due to the interference between two or more discrete bundles of rays or, equivalently, rays arriving from multiple images on the sky (Cordes & Wolszczan 1986; Wolszczan & Cordes 1987; Gupta, Bhat, & Rao 1999; Rickett, Lyne, & Gupta 1997, hereafter RLG).

A less well studied pattern in pulsar dynamic spectra consists of a crisscross of intensity maxima that are variably spaced perpendicular to the ridge lines of the maxima. Cordes & Wolszczan (1986) drew attention to these “multiple drift rates” in dynamic spectra, building on earlier work (Hewish 1980; Roberts & Ables 1982; Hewish, Wolszczan, & Graham 1985; Cordes et al. 1985). Numerous examples of the phenomenon are evident in the dynamic spectra presented by Gupta, Rickett, & Lyne (1994) in their multiyear study of eight pulsars, but the autocorrelation analysis that they employed is not well suited to its full elucidation. The remarkable episode of “fringing” in the dynamic spectra of PSR B0834+06 that RLG explore is also accompanied at all epochs by this phenomenon.

The central result of our study is to show that this crisscross pattern has a much clearer representation in transform space, where it is seen to be a high- Q phenomenon with a characteristic parabolic curvature. We discuss the constraints that the

presence of this pattern places on the image geometry and speculate on the physical structures that might give rise to this scattering geometry.

2. OBSERVATIONS AND DATA ANALYSIS

Our observations were made at the Arecibo Observatory³ at 430 MHz. Spectra across a 10 MHz band centered on this frequency were produced by a Fourier transform-based spectrometer (AOFTM⁴). Right- and left-circularly polarized signals were summed in hardware, and spectra with 1024 frequency channels (i.e., 10 kHz frequency resolution) were produced every ≈ 1.6 ms. During later analysis the spectra were synchronously averaged at the pulsar period, calculated using TEMPO (Taylor & Weisberg 1989), and summed over 10 s time intervals, creating a cube with axes of time, frequency, and pulsar rotational phase. We used 512 phase bins across the pulsar period. Dynamic spectra were created by producing an on-pulse spectrum from a window of phase bins centered on the pulse and subtracting an off-pulse spectrum to remove the baseline.

We observed 19 pulsars during 1999 January and 11 pulsars during 2000 January. A typical observation lasted 1 hr; we made 46 and 43 separate observations at the two observing epochs, respectively. Following several previous studies (e.g., Cordes & Wolszczan 1986; RLG), we produced two-dimensional power spectra from the dynamic spectra. These “secondary spectra” form the basis for most of the further analysis reported here. We normalized each secondary spectrum by its maximum and converted the relative power levels into a decibel scale.

Figure 1 shows dynamic and secondary spectra for PSR B0834+06. The crisscross pattern in the dynamic spectrum shows up in the secondary spectrum as two parabolic features, curving away from the conjugate time axis, that we call “arcs.” These arcs are remarkable for their narrowness and extent. In

¹ Department of Physics, Oberlin College, Oberlin, OH 44074.

² Department of Astronomy and Space Sciences Center, Cornell University, 512 Space Sciences Building, Ithaca, NY 14853.

³ The Arecibo Observatory is part of the National Astronomy and Ionosphere Center, which is operated by Cornell University under a cooperative agreement with the National Science Foundation.

⁴ See <http://www.naic.edu/~aofm>.

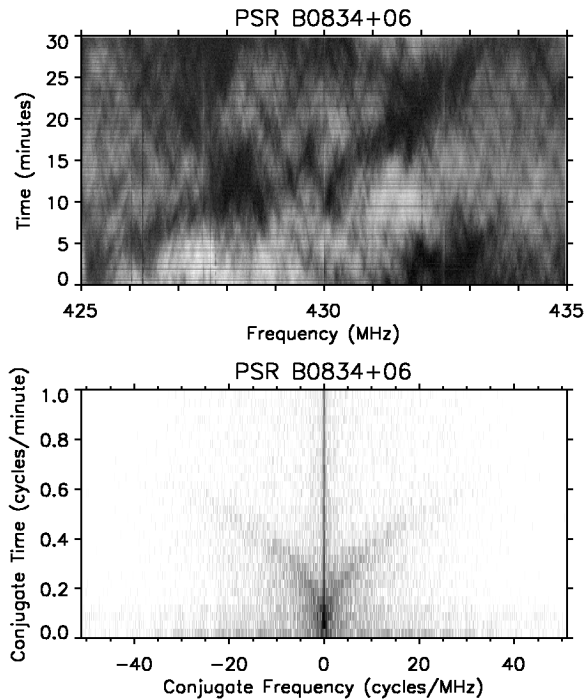


FIG. 1.—Dynamic spectrum (*top*) and its secondary spectrum for a 30 minute observation of PSR B0834+06 on 2000 January 18. The flux density is displayed as a linear gray scale with black indicating highest flux. The Nyquist limit along the vertical axis of the secondary spectrum is 3 cycles minute⁻¹, but the spectrum is noiselike beyond the region shown. The gray scale is logarithmic (linear in decibels), with the white level set 3 dB above the noise and the black level set 5 dB below the maximum array value at the origin, as in RLG. These limits span a 48 dB range. The strong vertical line in the center of the plot is due partly to the sidelobe response of the Fourier transform and partly to broadband pulse-to-pulse fluctuations that are only moderately quenched by the 10 s averaging interval. A similar horizontal line is due primarily to the sidelobe response.

Figure 2 we present secondary spectra, averaged over multiple days to improve dynamic range. PSR B0823+26 and PSR B0834+06 showed a persistent arc pattern over both the 1999 and 2000 observing runs. In 2000, PSR B0919+06 showed arcs that were relatively broad and faint and, hence, showed up only upon averaging of several secondary spectra. However, we did not see arcs in two high-quality 1999 observations. PSR B1133+16 showed arcs during most of the 1999 and 2000 observations, but several high-quality 2000 observations failed to show them, even though they were made on days adjacent to those on which they were present. PSR B1933+16 did not show the arc pattern in either of two high-quality observations in 1999 or 2000. Time variability of the arcs will be the subject of a separate study.

3. RESULTS

We detected arcs in the secondary spectra of pulsars B0823+26, B0834+06, B0919+06, and B1133+16. By using the relationship between fringe frequencies in the secondary spectrum and scattering parameters (e.g., Cordes & Wolszczan 1986; RLG; Gupta et al. 1999), we can analyze the arcs more quantitatively. Here we summarize a more detailed study that will be reported elsewhere (J. M. Cordes et al. 2001, in preparation). To simplify calculations, these treatments assume that the scattering takes place in a thin screen a distance D_s from the pulsar, with the pulsar-observer distance D . They show that

the interference between two points $\theta_{1,2}$ on the image plane (i.e., as seen by an observer) will lead to two-dimensional fringing in the dynamic spectrum with fringe frequencies

$$f_i = \frac{D}{\lambda D_s} (\theta_2 - \theta_1) \cdot \mathbf{V}_{\text{eff}, \perp}, \quad (1)$$

$$f_v = \frac{D}{2cD_s} (D - D_s)(\theta_2^2 - \theta_1^2). \quad (2)$$

Here f_i is the conjugate time axis, f_v is the conjugate frequency axis, and the effective velocity (Cordes & Rickett 1998) is a weighted sum of the velocities of the source, screen, and observer,

$$\mathbf{V}_{\text{eff}, \perp} = (1 - D_s/D)\mathbf{V}_{p \perp} + (D_s/D)\mathbf{V}_{\text{obs} \perp} - \mathbf{V}_{\text{screen} \perp}. \quad (3)$$

We can introduce the dimensionless variables

$$p = (\theta_2^2 - \theta_1^2) = \left[\frac{2cD_s}{D(D - D_s)} \right] f_v, \quad (4)$$

$$q = (\theta_2 - \theta_1) \cdot \hat{\mathbf{V}}_{\text{eff}, \perp} = \left(\frac{\lambda D_s}{D V_{\text{eff}, \perp}} \right) f_i, \quad (5)$$

where $\hat{\mathbf{V}}_{\text{eff}, \perp}$ is a two-dimensional unit vector for the effective velocity. Since p is quadratic in image angles and q is linear in image angles, p will generally be quadratic in q . This is essential to explaining the parabolic curvature of the arcs.

If we make the reasonable assumption that the pulsar velocity is much greater than either the velocity of the Earth or the screen, equations (4) and (5) can be simplified to

$$p = \left[\frac{2cs}{D(1-s)} \right] f_v, \quad (6)$$

$$q = \left[\frac{\lambda s}{V_{\text{pm}}(1-s)} \right] f_i, \quad (7)$$

where $s \equiv D_s/D$, and we approximate $V_{\text{eff}, \perp}$ by the measured proper motion speed, $V_{\text{pm}} = \mu D$. A parabolic arc ($p = q^2$) in the p - q plane then corresponds to a feature in the secondary spectrum of curvature

$$f_v = \frac{D}{2c} \frac{\lambda^2}{V_{\text{pm}}^2} \left(\frac{s}{1-s} \right) f_i^2. \quad (8)$$

In this model, the curvature of the arcs is determined solely by the screen placement, the pulsar distance, and the pulsar proper motion. Thus, by measuring the curvature of the arcs in the secondary spectrum, we can determine a value for the screen placement that is consistent with the observations and assumed values of D and V_{pm} , as in Table 1.

Gupta (1995) used diffractive bandwidth and timescale measurements to determine V_{iss} , the speed of the scintillation pattern past the observer (Cordes & Rickett 1998). Assuming that the scattering is dominated by a thin screen, one can determine the screen placement for which V_{iss} is consistent with V_{pm} . This is determined from Gupta's R_1 parameter by $s_{\text{iss}} = R_1^2/(1 + R_1^2)$. Table 1 shows that the values of s_{iss} agree well with those for s_{arc} , calculated with equation (8). Although the values of s_{iss} agree well with those for s_{arc} , the agreement may be fortuitous because there are significant uncertainties in both

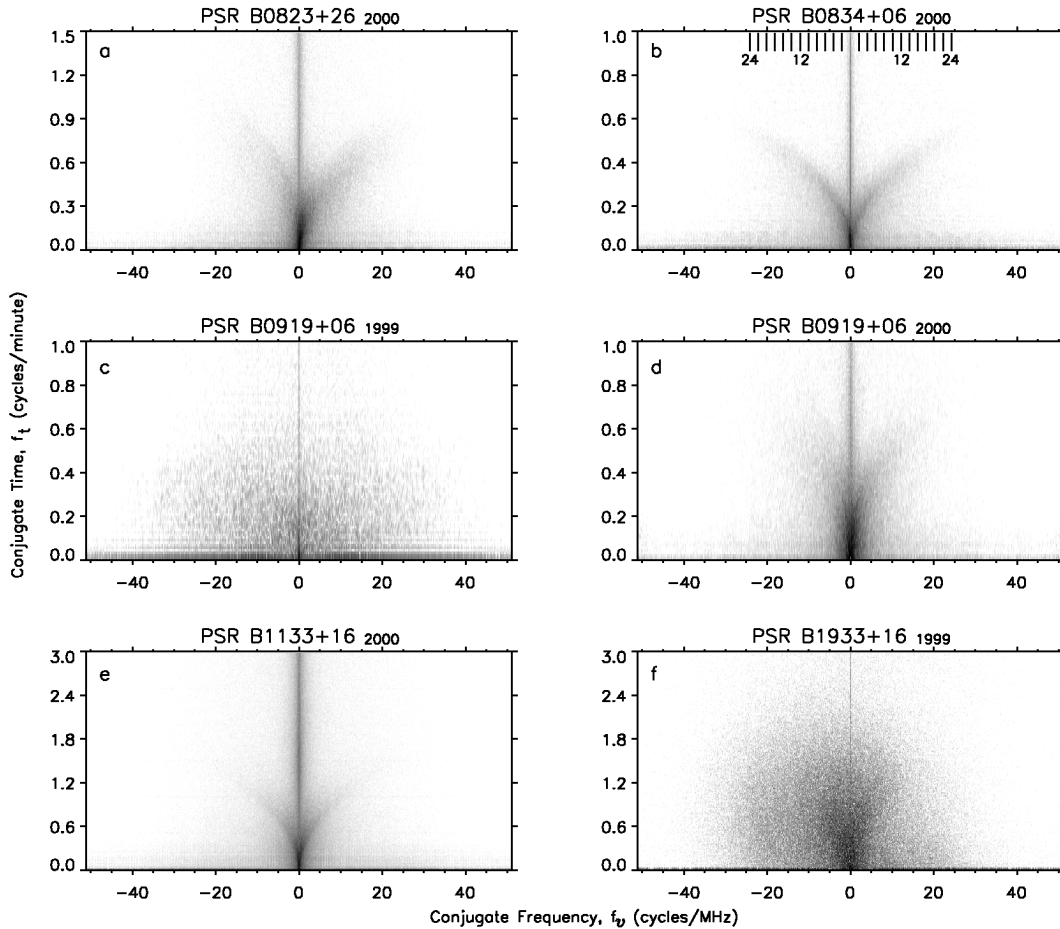


FIG. 2.—Co-added secondary spectra for five pulsars. The logarithmic gray scale is set as in Fig. 1. Only a portion of the conjugate time axis is shown in several cases. The range of displayed values is 49, 52, 48, 44, 56, and 39 dB for (a)–(f), respectively: (c) and (d) illustrate the time variability of the arcs; (f) is an example of a strong pulsar that does not display arcs.

the distances and the interstellar scintillation parameters used by Gupta; also, scattering is likely to receive contributions from the distributed ISM as well as from a screen. In particular, a recent study of B0919+06 (Chatterjee et al. 2001) that compares scintillation velocity estimates, which are epoch dependent, and the parallax and proper motion determined from Very Long Baseline Array observations finds that a thin screen must be combined with a distributed medium such as that of the Taylor & Cordes (1993) model to bring agreement between the two velocity estimates. At some epochs, the screen evidently causes multiple imaging of the pulsar.

From equation (1) it can be seen that the vertical (f_i) extent of arc features in the secondary spectrum is related to the angular extent of the scattering image along the effective ve-

locity vector. Table 1 shows the typical angular extent of the filament, $\theta_{x, \text{typ}}$, and the corresponding linear size on the screen, x_{typ} , inferred from the value of f_i for a generic model.

We analyze the distribution of power in the secondary spectrum with a sequence of vertical cuts, as in Figure 3. The rapid decline of power above the arcs strongly limits the image geometries that are consistent with the data. In order to exclude power above the arc, points must satisfy $p \geq q^2$. Referring to equations (4)–(5), this constraint can be expressed as

$$\theta_2^2 - \theta_1^2 \geq (\theta_{2x} - \theta_{1x})^2, \quad (9)$$

where the x -components are along the effective velocity vector. A single extended image has many image pairs that violate this

TABLE 1
SCATTERING SCREEN LOCATION

Pulsar	Distance (kpc)	V_{pm} (km s^{-1})	$f_{i, \text{arc}}$ (MHz^{-1})	$f_{i, \text{arc}}$ (minute^{-1})	s_{arc}	s_{iss}	$\theta_{x, \text{typ}}$ (mas)	x_{typ}
B0823+26	0.38	196	26	0.8	0.36	0.40	5.4	1.3
B0834+06	0.72	174	31	0.6	0.33	0.36	4.0	1.9
B0919+06	1.2	505	15	0.55	0.59	0.63	3.6	1.8
B1133+16	0.27	475	11	1.15	0.49	0.46	5.4	0.7

NOTE.—Values are derived from the Taylor & Cordes (1993) distance model and the Harrison, Lyne, & Anderson (1993) proper motions, except for recent interferometric results for PSR B0919+06 (Chatterjee et al. 2001).

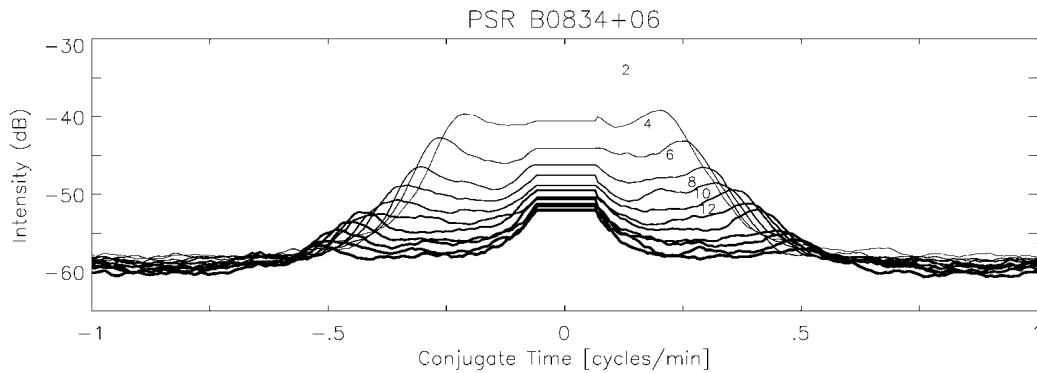


FIG. 3.—Cross-sectional cuts through the secondary spectrum of Fig. 2*b*, which was first smoothed by 1 cycle MHz^{-1} and $0.06 \text{ cycles minute}^{-1}$ (10×10 pixels). As shown by the tick marks in Fig. 2*b*, the cuts are taken parallel to the vertical axis at steps of $2 \text{ cycles MHz}^{-1}$. The cuts are made by reflecting the second quadrant of the secondary spectrum through the origin into the fourth quadrant and then cutting vertically along the conjugate time axis. The region near where the cuts cross $f_c = 0$ has been set to a constant value since the sidelobes rise to about -10 dB there. Only the first six cuts are labeled. Salient features are the similar height of the arcs on both sides of the origin, the sharp drop-off of power above the arcs (i.e., $|f_c| \geq 0.5$; note the logarithmic axis), the nearly constant power level below the arcs, and the low value of the noise floor.

condition and, hence, will produce a large amount of power above the arcs, inconsistent with the behavior seen. Hence, a multiple-image geometry is required to produce the clearly delineated arcs we observe.

One configuration that satisfies equation (9), having no detectable power above the arcs, consists of a bright pointlike image at the origin (direct line of sight to the pulsar) and a faint secondary image as a filled halo around it. The interference between a point at the origin and any other image point cannot produce power above the arcs because $\theta_1 = 0$. If the pointlike image and halo have maximum intensities proportional to a and b , respectively, then the pointlike source will produce a pointlike feature at the origin of the secondary spectrum with power proportional to a^2 (e.g., Cordes & Wolszczan 1986). The interimage interference between the point source and the halo will produce power proportional to ab . The self-interference between regions of the halo (which will produce power above the arcs) will be proportional to b^2 . Since this is smaller by another factor of b/a from the interimage term, then, for small b/a , the only detectable power will be a point source at the origin and power below the arcs.

Although the point source plus halo model is consistent with the observations, the scattering material in the screen would need to be inhomogeneous enough that the direct image of the pulsar would shine through, but rays slightly off-axis would be scattered. In essence, we would need to be seeing the pulsar through a break in the interstellar “clouds,” consistent with the

time variability of the arcs. On the other hand, there is strong evidence for scattering geometries based on filamentary structures (Rickett 1990). However, the self-interference between filaments will lead to features that are inconsistent with our data. Any viable model based on filamentary features in the image plane must somehow hide these self-interference features as well as produce the observed parabolic arcs.

The formalism used here includes only geometric delays, whereas differential dispersive delays may be important in some cases. The fact that the observed arcs conform to the geometric-only formalism implies that at least in some instances the dispersive effects are small. We have examples of secondary spectra that show more complex behavior and will analyze them within the more general framework in a later paper. An extended medium, as opposed to a single screen, also will be explored.

While there are many possibilities for source geometries, it is clear that a multicomponent scattered image is necessary. In future papers, we will apply this method to better understand the structure of the ISM on small spatial scales.

We thank T. Joseph Lazio for helpful discussions, the operators at Arecibo for help with remote observations, and Duncan Lorimer for the development of an excellent remote observing interface. We acknowledge support from the National Science Foundation: grant AST 96-18408 to J. M. C. and grant AST 96-19493 to D. R. S.

REFERENCES

- Chatterjee, S., Cordes, J. M., Lazio, T. J. W., Goss, W. M., Fomalont, E. B., & Benson, J. M. 2001, *ApJ*, in press
 Cordes, J. M., & Rickett, B. J. 1998, *ApJ*, 507, 846
 Cordes, J. M., Weisberg, J. M., & Boriakoff, V. 1985, *ApJ*, 288, 221
 Cordes, J. M., & Wolszczan, A. 1986, *ApJ*, 307, L27
 Gupta, Y. 1995, *ApJ*, 451, 717
 Gupta, Y., Bhat, N. D. R., & Rao, A. P. 1999, *ApJ*, 520, 173
 Gupta, Y., Rickett, B. J., & Lyne, A. G. 1994, *MNRAS*, 269, 1035
 Harrison, P. A., Lyne, A. G., & Anderson, B. 1993, *MNRAS*, 261, 113
 Hewish, A. 1980, *MNRAS*, 192, 799
 Hewish, A., Wolszczan, A., & Graham, D. A. 1985, *MNRAS*, 213, 167
 Rickett, B. J. 1990, *ARA&A*, 28, 561
 Rickett, B. J., Lyne, A. G., & Gupta, Y. 1997, *MNRAS*, 287, 739 (RLG)
 Roberts, J. A., & Ables, J. G. 1982, *MNRAS*, 201, 1119
 Scheuer, P. A. G. 1968, *Nature*, 218, 920
 Taylor, J. H., & Cordes, J. M. 1993, *ApJ*, 411, 674
 Taylor, J. H., & Weisberg, J. M. 1989, *ApJ*, 345, 434
 Wolszczan, A., & Cordes, J. M. 1987, *ApJ*, 320, L35